

Study of Ultrawide-Band Transmission in the Extremely High Frequency (EHF) Band

Yosef Pinhasi, Asher Yahalom, Oren Harpaz, and Guy Vilner

Abstract—The growing demand for broad-band wireless communication links and the lack of wide frequency bands within the conventional spectrum, causes us to seek bandwidth in the higher microwave and millimeter-wave spectrum at extremely high frequencies (EHF) above 30 GHz. One of the principal challenges in realizing modern wireless communication links in the EHF band are phenomena occurring during electromagnetic wave propagation through the atmosphere. A space-frequency approach for analyzing wireless communication channels operating in the EHF band is presented. Propagation of the electromagnetic radiation is studied in the frequency domain, enabling consideration of ultrawide-band modulated signals. The theory is employed for the analysis of a communication channel operating at EHF which utilizes pulse amplitude modulated signals. The atmospheric absorptive and dispersive effects on pulse propagation delay, pulse width and distortion are discussed. The theory and model are demonstrated in a study of ultrashort-pulse transmission at 60 GHz.

Index Terms—Atmospheric attention, millimeter wave propagation, ultrashort pulses, ultrawide-band transmission.

I. INTRODUCTION

THE growing demand for broad-band wireless communication links and the deficiency of wide frequency bands within the conventional spectrum, require utilization of higher microwave and millimeter-wave spectrum at the extremely high frequencies (EHF) above 30 GHz. In addition to the fact that the EHF band (30–300 GHz) covers a wide range, which is relatively free of spectrum users, it offers many advantages for wireless communication and RADAR systems as follows:

- broad bandwidths for high data rate information transfer;
- high directivity and spatial resolution;
- low transmission power (due to high antenna gain);
- low probability of interference/interception (due to narrow antenna beamwidths);
- small antenna and equipment size;
- no multipath fading (although fading can be caused by atmospheric conditions).

Among the practical advantages of using the EHF region for satellite communications systems is the ability to employ

smaller transmitting and receiving antennas. This allows the use of a smaller satellite and a lighter launch vehicle.

Some of the principal challenges in realizing modern wireless communication links at the EHF band are the effects emerging when the electromagnetic radiation propagates through the atmosphere. Fig. 1 is a schematic illustration of a wireless communication line-of-sight (LOS) link, where the distance between the transmitter and receiver sites is d .

At frequencies below the EHF band, the ratio between the received power P_r and the transmitted power P_t in line-of-sight (LOS) radio links, operating at a frequency f , is given by the well-known Friss transmission (“link budget”) formula [1], [2]

$$\frac{P_r}{P_t} = G_t \cdot \left(\frac{c}{4\pi \cdot f \cdot d} \right)^2 \cdot G_r \quad (1)$$

where G_t and G_r are the transmitting and receiving antenna gains respectively, and $c \cong 3 \cdot 10^8$ m/s is the speed of light. The above formula describes the “free-space loss” due to diffraction of the transmitted radiation without considering atmospheric attenuation due to absorption and scattering and ignores multipath effects along the path of propagation.

When millimeter-wave radiation passes through the atmosphere, it suffers from selective molecular absorption [3]–[8]. Several empirical and analytical models were suggested for estimating the millimeter and infrared wave transmission of the atmospheric medium. The transmission characteristics of the atmosphere at the EHF band, as shown in Fig. 3 was calculated with the millimeter propagation model (MPM), developed by Liebe [9], [10]. Curves are drawn for several values of relative-humidity (RH), assuming clear sky and no rain. Inspection of Fig. 3(a) reveals absorption peaks at 22 and 183 GHz, where resonance absorption of water (H_2O) occurs, as well as absorption peaks at 60 and 119 GHz, due to absorption resonances of oxygen (O_2). Between these frequencies, minimum attenuation is obtained at 35 (*Ka* band), 94 (*W* band), 130, and 220 GHz, which are known as atmospheric transmission “windows” [6].

The transmission characteristics are determined by weather conditions such as temperature, pressure and humidity. The absorption is proportional to air density, and thus reduces with height. Attenuation due to fog, haze, clouds, rain and snow is one of the dominant causes of fading in wireless communication links operating in the EHF band [11], [12]. Raindrops and dust scatter millimeter wave radiation, resulting in amplitude fluctuations and phase randomness in the received signal. This further degrades the availability and performance of the communication links. Sufficient fade margins are essential for a reliable system.

The inhomogeneous transmission in a band of frequencies causes absorptive and dispersive effects in the amplitude and in phase of wide-band signals transmitted in the EHF band.

Manuscript received July 27, 2003; revised February 13, 2004. This work was supported by the Israeli Software Radio Consortium, supported by the MAGNET program of the State of Israel Ministry of Industry and Commerce.

Y. Pinhasi, A. Yahalom, and O. Harpaz are with the Department of Electrical and Electronic Engineering, The College of Judea and Samaria, Ariel 44837, Israel (e-mail: yosip@eng.tau.ac.il).

G. Vilner was with the Department of Electrical and Electronic Engineering, The College of Judea and Samaria, Ariel 44837, Israel. He is now a private contractor.

Digital Object Identifier 10.1109/TAP.2004.835121

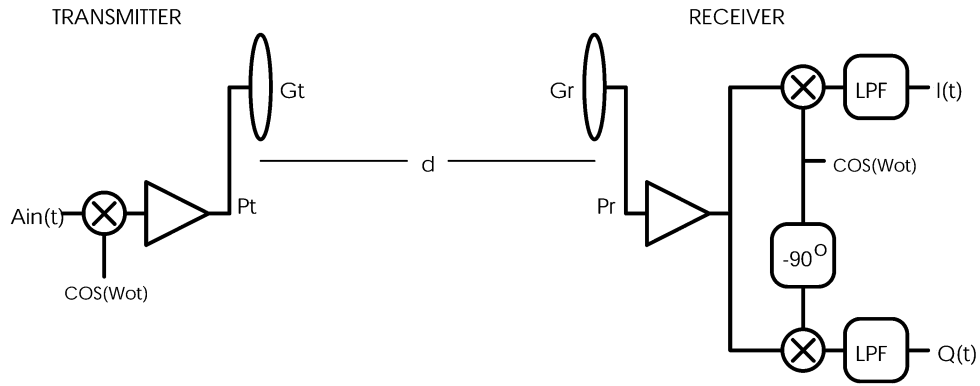


Fig. 1. Wireless line-of-sight communication link.

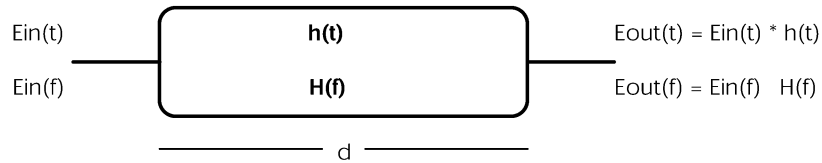


Fig. 2. Linear system representing propagation of electromagnetic waves in a medium.

The frequency response of the atmosphere plays a significant role as the data rate of a wireless digital radio channel is increased. The resulting amplitude and phase distortion leads to inter-symbol interference, and thus to an increase in the bit error rate (BER). These effects should be taken into account in the design of broad-band communication systems, including careful consideration of appropriate modulation, equalization and multiplexing techniques.

Several theoretical papers dealt with the problem of distortion occurring when a short pulse is propagating in absorptive and dispersive media, including gases and plasmas [13]–[19]. They also studied the delay and pulse shape evolution along the path of propagation. Gibbins [18] extended earlier investigations [14], [16] and examined distortions of short Gaussian pulses, modulating millimeter waves and propagating in the atmosphere. An approximation of the wave propagation factor was used to derive analytical expressions for the pulse shape. Conditions for pulse broadening and compression were identified.

Approximate formulations are restricted to an initial Gaussian pulse and result in errors in the calculation of its shape evolution during propagation. These errors increase as the initial pulse duration is shortened. Moreover, the validity of the analytical expression is limited, and does not permit consideration of ultrashort pulses, which violate the conditions for existence of a solution. In this paper, we develop a general space-frequency approach for studying wireless communication channels operating in the EHF band. The theory is used to compare between analytical and numerical models. The constraints of the derived analytical expressions are discussed, pointing out conditions of validity. The MPM model [9], [10] is used in the numerical model for calculation of atmospheric characteristics in the frequency domain. The resulting propagation factor is calculated numerically, enabling one to deal with ultrawide-band arbitrary signals.

The theory was used to study the effects of the atmospheric medium on a radio link, shown in Fig. 1. The data signal, represented by a complex envelope $A_{in}(t)$, modulates a carrier wave

at frequency f_0 . The resultant signal is transmitted and propagates to the receiver site through the atmosphere along a line-of-sight path. The demodulated in-phase $I_{out}(t)$ and quadrature $Q_{out}(t)$ signals, retrieved at the receive outputs, are examined allowing evaluation of the performance of a high data rate digital wireless channel operating at millimeter wavelengths.

The application of the model is demonstrated on a wireless data link operating in the 60 GHz band. The unused frequency space and the high attenuation due to oxygen absorption (-15 dB/Km) [20]–[22] make this frequency range naturally fitting for local broad-band digital networks with small reuse distances [23]. The effects predicted by the analytical derivations are inspected in the numerical simulations, including the evolution of pulse distortion along the path of propagation in the atmospheric medium. The numerical model enables consideration of further ultrashort pulses, enduring very few carrier periods; such situations cannot be treated with the aid of analytical approximated derivations.

II. MILLIMETER WAVE PROPAGATION IN THE ATMOSPHERE

The time dependent field $E(t)$ represents an electromagnetic wave propagating in a medium. The Fourier transform of the field is

$$\mathbf{E}(f) = \int_{-\infty}^{+\infty} E(t) \cdot e^{-j2\pi ft} dt. \quad (2)$$

Propagation of electromagnetic waves in a medium can be viewed as transformation through a system (see Fig. 2).

In the far field, transmission of a wave, radiated from a localized (point) isotropic source and propagating in a (homogeneous) medium is characterized in the frequency domain by the transfer function, derived in Appendix A

$$H(f) \equiv \frac{\mathbf{E}_{out}(f)}{\mathbf{E}_{in}(f)} = \frac{d_0}{d_0 + d} \cdot e^{-jk(f) \cdot d}. \quad (3)$$

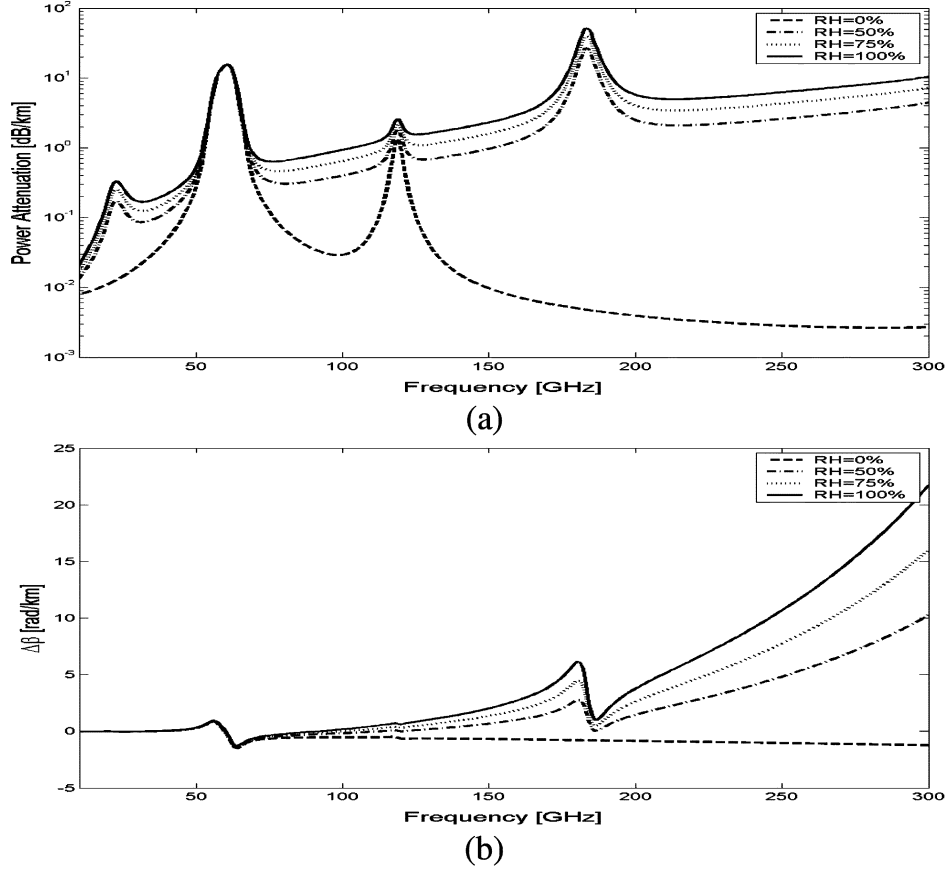


Fig. 3. Millimeter wave (a) attenuation coefficient $20 \log(e) \cdot \alpha(f)$ in [dB/Km] and (b) wavenumber increment $\Delta\beta(f) = (2\pi f/c) \cdot N_r(f)$ in [rad/Km] for various values of relative humidity (RH).

Here, $k(f) = 2\pi f \sqrt{\mu\epsilon}$ is a frequency dependent propagation factor, where ϵ and μ are the permittivity and the permeability of the medium, respectively. The transfer function $H(f)$ describes the frequency response of the medium. Its inverse Fourier transformation corresponds to the temporal impulse response $h(t)$. In a dielectric medium the permeability is equal to that of the vacuum $\mu = \mu_0$ and the permittivity is given by $\epsilon(f) = \epsilon_r(f) \cdot \epsilon_0$. If the medium introduces losses and dispersion, the relative dielectric constant $\epsilon_r(f)$ is a complex, frequency dependent function, for which its real and imaginary parts satisfy the Kramers-Kronig relations [24], [25]. The resulting index of refraction $n(f) = \sqrt{\epsilon_r(f)}$ can be presented by

$$n(f) = 1 + N(f) \quad (4)$$

where $N(f) = N_r(f) - j \cdot N_i(f)$ is the complex refractivity of the molecules composing the air [11]. The propagation factor can be written in terms of the index of refraction

$$k(f) = \frac{2\pi f}{c} \cdot n(f). \quad (5)$$

Substituting expressions (4) and (5) in (3), assuming horizontal propagation in an homogeneous medium, results in the transfer function

$$H(f) = \frac{d_0}{d_0 + d} \cdot e^{-[\alpha(f) + j\beta(f)] \cdot d} \quad (6)$$

where $\alpha(f) = -\text{Im}\{k(f)\} = (2\pi f/c) \cdot N_i(f)$ is the attenuation coefficient and $\beta(f) = \text{Re}\{k(f)\} = (2\pi f/c) \cdot [1 + N_r(f)]$ is the wavenumber of the propagating wave, shown in Fig. 3.

The power transfer function along the propagation path is given by

$$|H(f)|^2 = \left(\frac{d_0}{d_0 + d} \right)^2 \cdot e^{-2\alpha(f) \cdot d} \quad (7)$$

and is shown in Fig. 4 for frequencies of 35 and 94 GHz, where minimum attenuation (“transmission window”) is obtained, as well for 60 and 119 GHz where maximum absorption by oxygen molecules occurs.

III. TRANSMISSION OF BROAD-BAND MODULATED SIGNAL

Assume that a carrier wave at f_0 is modulated by a wide-band signal $A_{\text{in}}(t)$

$$E_{\text{in}}(t) = \text{Re}\{A_{\text{in}}(t) \cdot e^{j2\pi f_0 t}\} \quad (8)$$

as shown in Fig. 1. Here, $A_{\text{in}}(t) = I_{\text{in}}(t) - jQ_{\text{in}}(t)$ is a complex envelope, representing the base-band signal, where $I_{\text{in}}(t) = \text{Re}\{A_{\text{in}}(t)\}$ and $Q_{\text{in}}(t) = -\text{Im}\{A_{\text{in}}(t)\}$ are the in-phase and the quadrature information waveforms, respectively. The Fourier transform of the transmitted field is

$$\mathbf{E}_{\text{in}}(f) = \frac{1}{2} \mathbf{A}_{\text{in}}(f - f_0) + \frac{1}{2} \mathbf{A}_{\text{in}}^*[-(f + f_0)] \quad (9)$$

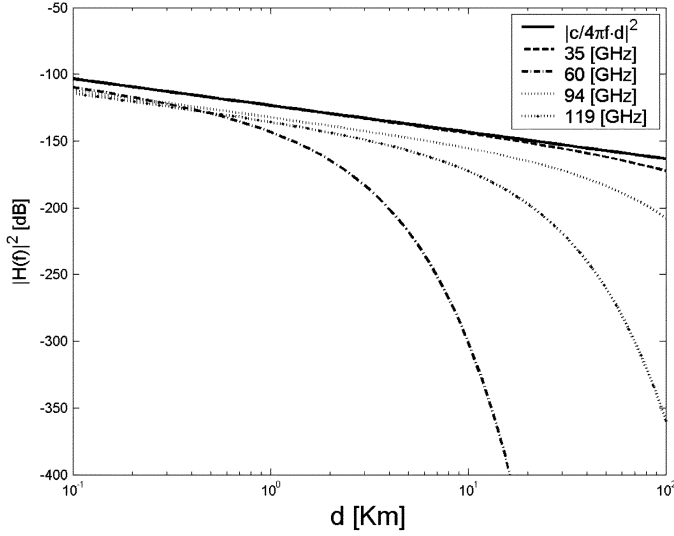


Fig. 4. Power transfer at the “transmission window” frequencies of 35 and 94 GHz and at the oxygen absorption frequencies of 60 and 119 GHz.

where $\mathbf{A}_{in}(f)$ is the Fourier transform of the complex envelope $A_{in}(t)$. After propagating along a path with a distance d , the field is

$$\mathbf{E}_{out}(f) = \frac{1}{2} \mathbf{A}_{in}(f - f_0) \cdot H(f) + \frac{1}{2} \mathbf{A}_{in}^*[-(f + f_0)] \cdot H^*(-f). \quad (10)$$

Since the transfer function $H(f)$ is the Fourier transform of a real function $H(f) = H^*(-f)$. The inverse Fourier transformation of (10), results in a received field given in the time domain by

$$E_{out}(t) = \text{Re}\{A_{out}(t) \cdot e^{j2\pi f_0 t}\} \quad (11)$$

where the complex envelope of the signal obtained at the receiver cite is given by

$$A_{out}(t) = \int_{-\infty}^{+\infty} \mathbf{A}_{in}(f) \cdot H(f + f_0) \cdot e^{+j2\pi f t} df. \quad (12)$$

The formalism developed above is utilized in the following for analytical derivation and numerical calculations of the demodulated signal at the receiver site. The flow chart in Fig. 5 summarizes the procedure carried out for solving (12). A base-band digital signal $A_{in}(t)$, fed to the modulator at the transmitter site modulates a carrier at f_0 . The MPM model [10]–[12] is called for to calculate the complex refractivity of the atmosphere, as required in the transfer function (6). Finally, the demodulated complex signal $A_{out}(t)$ and its related quadrature components $I_{out}(t)$ and $Q_{out}(t)$ obtained at the receiver output are found, employing an algorithm of fast Fourier transformation (FFT) for solving (12).

IV. ULTRAWIDE-BAND PULSE MODULATION

Assume that the transmitted waveform is a carrier modulated by a Gaussian envelope

$$A_{in}(t) = e^{-\frac{t^2}{2\sigma_{in}^2}} \quad (13)$$

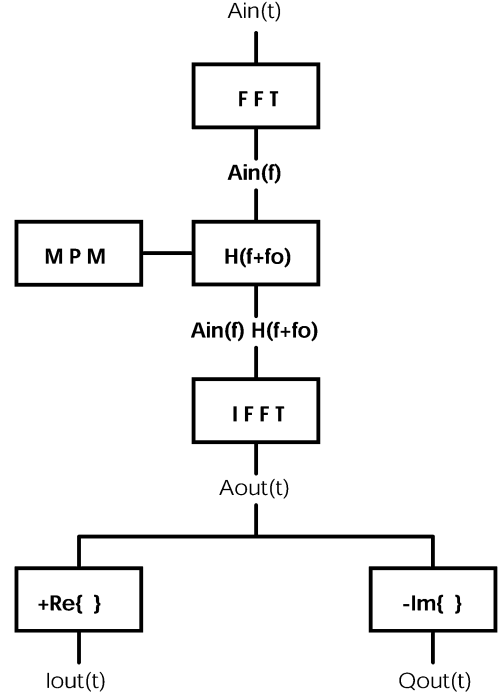


Fig. 5. Procedure for calculation of demodulated quadrature signals received in a wireless communication channel.

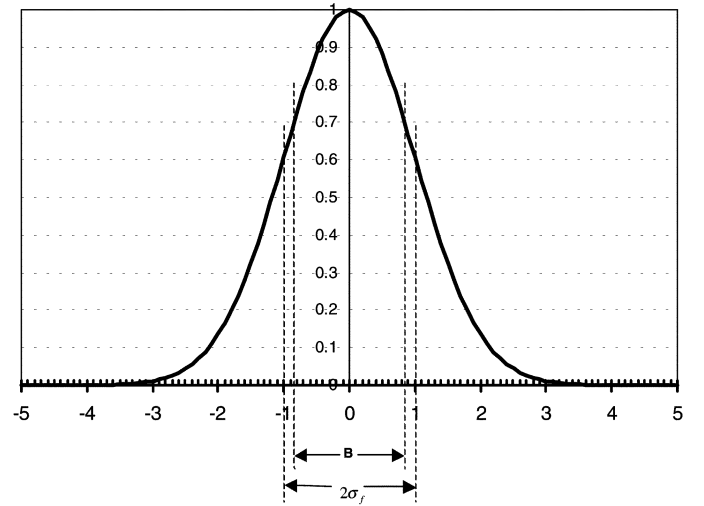


Fig. 6. Normalized Gaussian lineshape.

characterized by a standard deviation σ_{in} . Fourier transformation of the pulse results in a Gaussian line-shape in the frequency domain

$$\mathbf{A}_{in}(f) = \sqrt{2\pi} \cdot \sigma_{in} \cdot e^{-\frac{1}{2}(2\pi\sigma_{in}f)^2} \quad (14)$$

shown in Fig. 6. The corresponding standard deviation frequency bandwidth is $\sigma_f = (1)/(2\pi\sigma_{in})$. The full-width half-maximum (FWHM) is the -3 dB bandwidth and is equal to $B = 2 \cdot \sqrt{\ln(2)} \cdot \sigma_f \cong 0.265 \cdot \sigma_{in}^{-1}$.

In order to calculate the pulse shape $A_{out}(t)$ after propagation along a horizontal path in the atmospheric medium, we substitute the Fourier transform (14) into expression (12). Analytical result can be found if the complex propagation factor (5) is

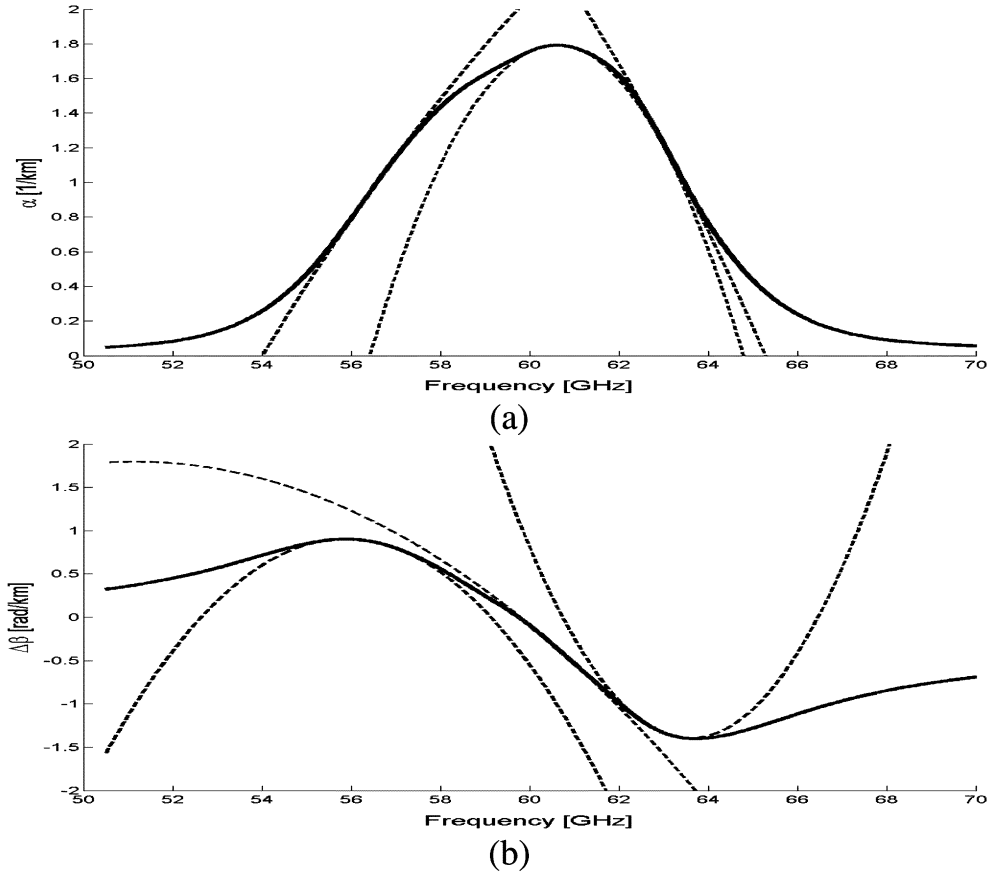


Fig. 7. Absorption line of the Oxygen at 60 GHz (a) attenuation coefficient $\alpha(f) = (2\pi f/c) \cdot N_i(f)$ and (b) wavenumber increment $\Delta\beta(f) = (2\pi f/c) \cdot N_r(f)$.

TABLE I
COMPLEX PROPAGATION FACTORS AT THE 60 GHz BAND

Frequency:	56.5GHz	60.5GHz	63GHz
$jk = \alpha + j\beta$ [1/m]	$9.70 \cdot 10^{-4} + j \cdot 1.19 \cdot 10^{-3}$	$1.79 \cdot 10^{-3} + j \cdot 1.27 \cdot 10^{-3}$	$1.22 \cdot 10^{-3} + j \cdot 1.33 \cdot 10^{-3}$
$jk' = \alpha' + j\beta'$ [s/m]	$3.59 \cdot 10^{-13} + j \cdot 2.10 \cdot 10^{-8}$	$0 + j \cdot 2.10 \cdot 10^{-8}$	$-4.81 \cdot 10^{-13} + j \cdot 2.10 \cdot 10^{-8}$
$jk'' = \alpha'' + j\beta''$ [s ² /m]	$0 - j \cdot 1.70 \cdot 10^{-22}$	$-2.07 \cdot 10^{-22} - j \cdot 4.84 \cdot 10^{-23}$	$0 + j \cdot 3.39 \cdot 10^{-22}$

approximated in the vicinity of the carrier frequency f_0 , by a second-order Taylor expansion [14]–[16]

$$k(f) \cong k_0 + k' \cdot (f - f_0) + \frac{1}{2}k'' \cdot (f - f_0)^2 \quad (15)$$

where $k_0 \equiv k(f_0)$, $k' \equiv (dk/df)|_{f_0}$, $k'' \equiv (d^2k)/(df^2)|_{f_0}$. The second-order approximation given in (15) can be used if the standard deviation σ_{in} of the Gaussian pulse satisfies

$$\sum_{n=0}^2 \frac{1}{n!} \cdot k^{(n)} \cdot \sigma_{in}^{-n} \gg \sum_{n=3}^{\infty} \frac{1}{n!} \cdot k^{(n)} \cdot \sigma_{in}^{-n}$$

resulting in a complex envelope

$$A_{out}(t) = \frac{d_0}{d_0 + d} \cdot \frac{\sigma_{in}}{\sigma} \cdot e^{-\frac{(t - \frac{k'd}{2\pi})^2}{2\sigma^2}} \cdot e^{-jk_0 \cdot d} \quad (16)$$

where

$$\sigma^2 = \sigma_{in}^2 + j \frac{k''}{(2\pi)^2} \cdot d.$$

The expression obtained at (16) is valid if

$$\text{Re}\{\sigma^2\} = \sigma_{in}^2 + \frac{\alpha'' d}{(2\pi)^2} > 0. \quad (17)$$

This condition is always satisfied if $\alpha'' > 0$. However, at frequencies for which the attenuation curve is convex $\alpha'' < 0$ (in the vicinity of the absorption lines) the analytical results are valid only for $\sigma_{in}^2 > -(\alpha'' d / (2\pi)^2) > 0$. Another interpretation of this result is that for a given initial pulse width σ_{in} , the distance should not exceed $d < -((2\pi\sigma_{in})^2) / (\alpha'')$ in order for (16) to be valid.

The magnitude (absolute value) of the complex envelope given by (16), has a Gaussian shape

$$|A_{out}(t)| = \frac{d_0}{d_0 + d} \cdot \frac{\sigma_{in}}{|\sigma|} \cdot \exp\left[-\alpha_0 \cdot d + \frac{1}{2} \frac{(\alpha' d)^2}{(2\pi\sigma_{in})^2 + \alpha'' d}\right] \cdot e^{-\frac{(t - t_d)^2}{2\sigma_{out}^2}} \quad (18)$$

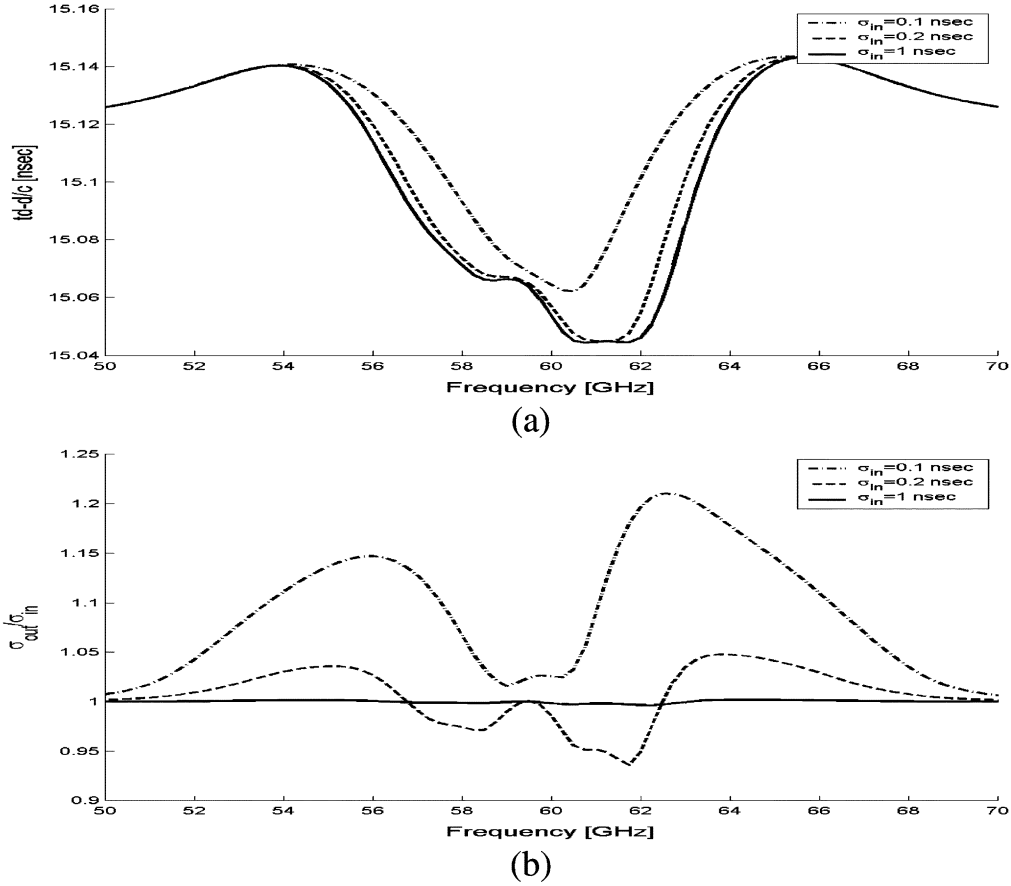


Fig. 8. Graphs of (a) group delay and (b) standard deviation versus frequency after a pulse propagation distance of $d = 1$ Km.

with a temporal delay

$$t_d = \frac{1}{2\pi} \left[\beta' - \frac{\alpha' \beta'' d}{(2\pi\sigma_{in})^2 + \alpha'' d} \right] \cdot d \quad (19)$$

and a standard deviation σ_{out} given by

$$\sigma_{out}^2 = \sigma_{in}^2 + \frac{\alpha'' d}{(2\pi)^2} + \frac{\left[\frac{\beta'' d}{(2\pi)^2} \right]^2}{\sigma_{in}^2 + \frac{\alpha'' d}{(2\pi)^2}} \cdot d \quad (20)$$

These results, which can be obtained from the solutions derived in [14] and [16], show that in the framework of the approximation (15), a Gaussian magnitude $|A_{out}(t)| = \sqrt{I_{out}^2(t) + Q_{out}^2(t)}$ is preserved while propagating in the medium (although its width changes) and thus can be retrieved by the receiver.

Since the pulse cannot propagate above a velocity of the speed of light the time delay, given by (19) is always $t_d > (d/c)$. This fact points out that the medium response should fulfill $\beta' - (\alpha' \beta'' / \alpha'') > (2\pi/c)$ at any frequency. For a short distance (or a wide pulse), the time delay can be approximated by $t_d \approx (\beta' / 2\pi) \cdot d$. This becomes the exact solution at attenuation peaks, where $\alpha' = 0$. When $\alpha'' < 0$, the denominator of (19) may become arbitrary small, (however should be kept positive in order to satisfy the validity condition (17)). In that case the time delay is approximately $t_d \approx -(1/2\pi)(\alpha' \beta'' d^2) / ((2\pi\sigma_{in})^2 + \alpha'' d)$ (where must be $\alpha' \beta'' < 0$), resulting in an arbitrary long delay in the pulse arrival at a distance d .

Examination of (20) reveals that when $\alpha'' \geq 0$ the pulse always widens along the path of propagation. However, for $\alpha'' < 0$ (e.g., in the vicinity of absorption frequencies), the pulse may become narrower while propagating in the atmospheric medium. Pulse compression occurs when $(\sigma_{in}^2) / (d) > -(1) / ((2\pi)^2 \alpha'') (\alpha''^2 + \beta''^2)$. In both cases minimum pulse width is obtained for $\sigma_{in}^2 = (d / (2\pi)^2) (|\beta''| - \alpha'')$ resulting in $\sigma_{out, min}^2 = 2(|\beta''| d) / ((2\pi)^2)$.

For long propagation distances, the time delay approaches $t_d \rightarrow (1/2\pi \alpha'') (\alpha'' \beta' - \alpha' \beta'') \cdot d$ and the standard deviation $\sigma_{out}^2 \rightarrow (1/(2\pi)^2) \alpha'' (\alpha''^2 + \beta''^2) \cdot d$.

V. NUMERICAL RESULTS—PROPAGATION AT 60 GHz

An interesting application of the described approach is the analysis of transmission of ultrashort-pulses in the 60 GHz band. The high atmospheric attenuation and dispersive effects, caused by the absorption of the oxygen molecules at this frequency region [23]–[25], are expressed as evident distortions on the pulse delay, duration and shape. The complex propagation factor $jk(f) = \alpha(f) + j\beta(f)$ in the 60 GHz band is shown in Fig. 7 as a solid line. The dashed lines describe curves of polynomials, which resulted from second-order Taylor expansions at 60.5 GHz, where the absorption peaks ($\alpha' = 0$) and at 56.5 and 63 GHz, where $\alpha'' = 0$.

Table I summarizes the values of the complex propagation factor at these three frequencies, including their first and second derivatives. These numbers are used in the analytical

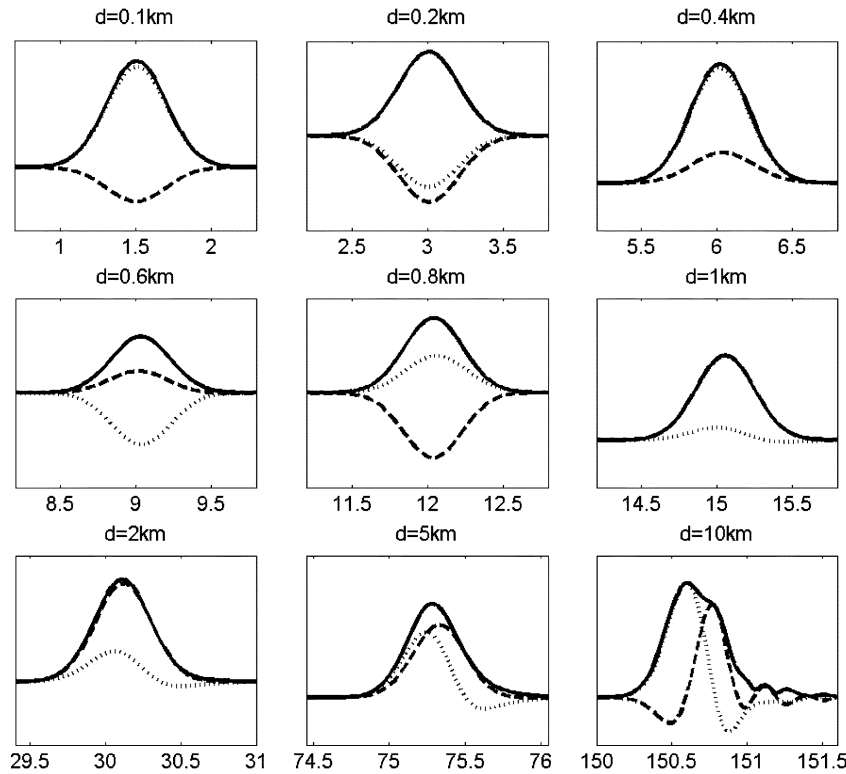


Fig. 9. Pulse amplitude $|A_{out}(t)|$ (solid line) and its corresponding quadrature $I_{out}(t)$ (dashed line) and $Q_{out}(t)$ (dotted line) components along the path of propagation. The time axis is of $t - (d/c)$ in [nanosecond].

investigation of the delay (19) and pulse width (20) of a pulse modulated signal transmitted through the atmosphere.

The procedure, following the flow chart of Fig. 5, was employed in a numerical program aimed at the simulation of pulse transmission in the atmosphere. In our study, the modulating base-band signal $A_{in}(t)$ was taken to be Gaussian, as given in (13). The initial standard deviation σ_{in} of pulse duration was varied, examining its effect on the resultant pulse envelope $A_{out}(t)$ along the path of propagation. It calculates the n th order “moments” of the temporal magnitude of the envelope $|A_{out}(t)|$

$$\bar{t}^n = \frac{\int_{-\infty}^{+\infty} t^n \cdot |A_{out}(t)| dt}{\int_{-\infty}^{+\infty} |A_{out}(t)| dt}. \quad (21)$$

The first-order ($n = 1$) moment represents the delay of the pulse $\bar{t} \cong t_d$. Examination of the approximated analytical expression (19) derived in the preceding section, discloses that the first-order derivative α' of the attenuation coefficient plays a role in determining the pulse delay. Its major effect on increasing of the group delay is observed in Fig. 8(a) in the vicinity of the frequencies 56.5 and 63 GHz, where the most negative values of the product $\alpha'\beta''$ are obtained. Minimum delay is obtained at 60.5 GHz where $\alpha' = 0$ as expected by (19).

The standard deviation $\sigma_{out} = \sqrt{\bar{t}^2 - (\bar{t})^2}$ represents the typical width of the pulse at the receiver output. Its frequency dependent behavior is shown in Fig. 8(b) for several initial pulse widths σ_{in} . In this example, a pulse with initial duration of

$\sigma_{in} = 0.2$ ns is shown to be shortened ($(\sigma_{out})/(\sigma_{in}) < 1$) at frequencies where $\alpha'' < 0$, satisfies conditions for compression resulting from (20).

Fig. 9 shows a set of pulse envelopes $|A_{out}(t)|$ obtained from numerical calculations for several distances along the propagation path (solid line). The quadrature components $I(t)$ and $Q(t)$ are also drawn. An initial Gaussian shape pulse with $\sigma_{in} = 0.2$ ns was assumed. Distortions in the shape increase as shown as the pulse propagates to long distances.

Curves of the group delay and standard deviation of the propagating pulse as a function of its initial width σ_{in} are drawn in Fig. 10 for the three frequencies discussed above. A minimum delay is observed in Fig. 10(a) at a carrier frequency of 60.5 GHz where the absorption peaks ($\alpha' = 0$), while higher delays are found at 56.5 and 63 GHz, where $\alpha'\beta''$ is negative. Fig. 9(b) shows the range of values of σ_{in} for which conditions for pulse compression occur at 60.5 GHz (where $\alpha'' < 0$).

VI. CONCLUSION

The space-frequency approach presented in this paper for the propagation of electromagnetic waves in dielectric media, enables consideration of the effects of the absorptive and dispersive characteristics of materials composing the media, on the transmission of wide-band signals. Using a complex representation of a frequency dependent refraction index, a transfer function that describes the frequency response of the medium is formulated.

Atmospheric transmission of millimeter waves, modulated by ultrashort Gaussian pulses, is studied analytically and

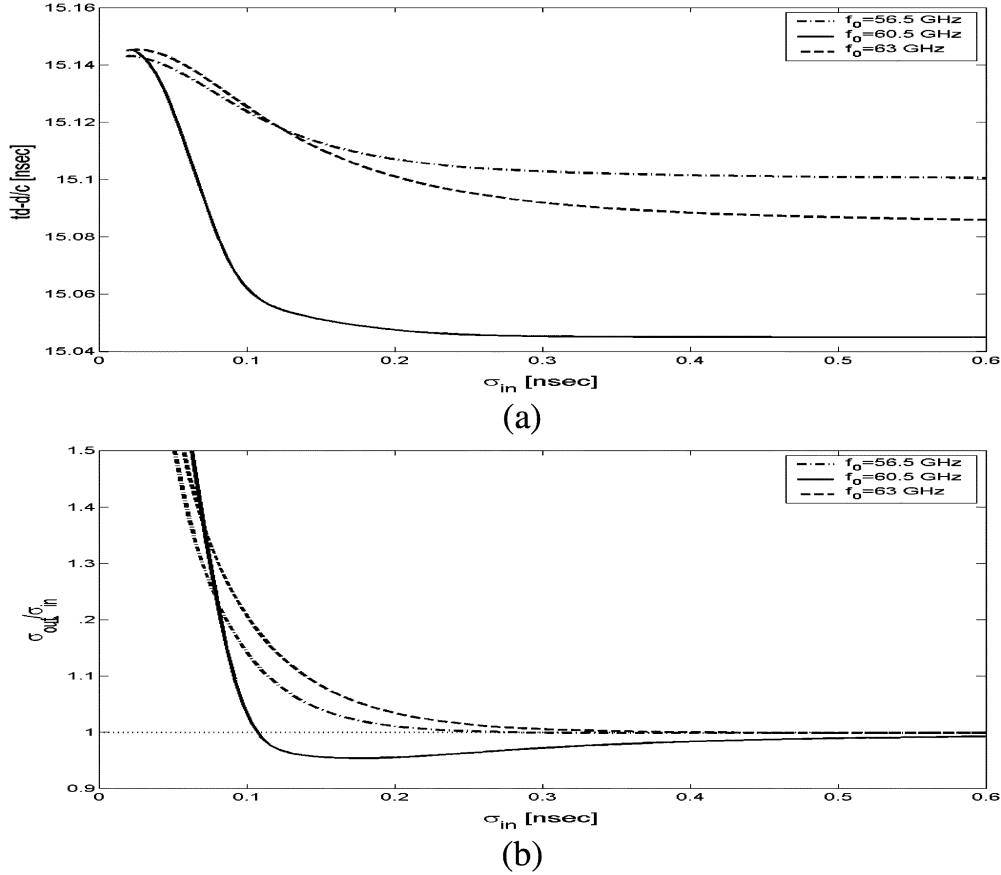


Fig. 10. Graphs of (a) group delay and (b) standard deviation as a function initial pulse duration, after a propagation distance of $d = 1$ Km.

numerically in the frequency domain revealing spectral effects on pulse propagation delay, width and distortions. Using second-order expansion of the propagation factors leads to the derivation of approximated analytical expressions for the delay and width as a function of distance and carrier frequency. Conditions under which pulse compression or expansion were identified. The analytical solution is found to be limited in describing wide-band communication links where ultrashort pulses are involved. In such links the numerical model use is required.

The effects, predicted by the analytical solution, were compared to the results obtained from a numerical simulation, aimed at the calculation of pulse evolution while propagating in the atmospheric media. By studying propagation of a pulse in the atmosphere, characterized by the millimeter-wave propagation model (MPM), it was shown that even in a medium of atmospheric air some of the effects that we predict are pronounced especially for carrier frequencies in the vicinity of the 60 GHz, where high absorption of oxygen molecules occurs.

APPENDIX A

This appendix is aimed at derivation of the transfer function given in (3). In an homogeneous dielectric medium, the electric $\mathbf{E}(\mathbf{r}, t)$ and magnetic $\mathbf{H}(\mathbf{r}, t)$ fields, excited by current $\mathbf{J}(\mathbf{r}, t)$

and charge $\rho(\mathbf{r}, t)$ densities, follow the macroscopic Maxwell equations, consisting of Faraday law

$$\nabla \times \mathbf{E}(\mathbf{r}, t) = -\frac{\partial}{\partial t} \mathbf{B}(\mathbf{r}, t) \quad (\text{A.1})$$

Ampere law

$$\nabla \times \mathbf{H}(\mathbf{r}, t) = \mathbf{J}(\mathbf{r}, t) + \frac{\partial}{\partial t} \mathbf{D}(\mathbf{r}, t) \quad (\text{A.2})$$

and Gauss laws

$$\begin{aligned} \nabla \cdot \mathbf{D}(\mathbf{r}, t) &= \rho(\mathbf{r}, t) \\ \nabla \cdot \mathbf{B}(\mathbf{r}, t) &= 0. \end{aligned} \quad (\text{A.3})$$

Here, $\mathbf{D}(\mathbf{r}, t)$ and $\mathbf{B}(\mathbf{r}, t)$ are the electric and magnetic flux densities respectively. In a homogeneous isotropic dielectric medium, their Fourier transforms can be written as $\tilde{\mathbf{D}}(\mathbf{r}, f) = \varepsilon(f)\tilde{\mathbf{E}}(\mathbf{r}, f)$ and $\tilde{\mathbf{B}}(\mathbf{r}, f) = \mu\tilde{\mathbf{H}}(\mathbf{r}, f)$, where $\varepsilon(f)$ is the frequency dependent permittivity and μ is the permeability of the medium. Substituting the last relations in the Fourier transform of the Maxwell equations results in a space-frequency Helmholtz equation

$$\begin{aligned} \nabla^2 \tilde{\mathbf{E}}(\mathbf{r}, f) + k^2(f)\tilde{\mathbf{E}}(\mathbf{r}, f) &= \frac{1}{\varepsilon} \nabla \tilde{\rho}(\mathbf{r}, f) \\ &\quad - j2\pi f \mu \cdot \tilde{\mathbf{J}}(\mathbf{r}, f) \end{aligned} \quad (\text{A.4})$$

where $k(f) = \sqrt{\mu\varepsilon(f)} \cdot 2\pi f$. Defining a driving term $\vec{F}(\mathbf{r}, f)$

$$-4\pi\vec{F}(\mathbf{r}, f) = \frac{1}{\varepsilon}\nabla\tilde{\rho}(\mathbf{r}, f) - j2\pi f\mu \cdot \tilde{\mathbf{J}}(\mathbf{r}, f) \quad (\text{A.5})$$

we obtain the equation in the form

$$\nabla^2\tilde{\mathbf{E}}(\mathbf{r}, f) + k^2(f)\tilde{\mathbf{E}}(\mathbf{r}, f) = -4\pi\vec{F}(\mathbf{r}, f). \quad (\text{A.6})$$

The Green function $G(\mathbf{r}, f)$ is the result of a point-source excitation

$$\nabla^2 G(\mathbf{r}, f) + k^2(f)G(\mathbf{r}, f) = -4\pi\delta(\mathbf{r} - \mathbf{r}'). \quad (\text{A.7})$$

This equation can be written in terms of $\mathbf{R} = \mathbf{r} - \mathbf{r}'$ as

$$\nabla_{\mathbf{R}}^2 G(\mathbf{r}, f) + k^2(f)G(\mathbf{r}, f) = -4\pi\delta(\mathbf{R}). \quad (\text{A.8})$$

Since the Green function must be spherically symmetric, the (A.9) can be written in the form

$$\frac{1}{R} \frac{d^2}{dR^2} [RG(\mathbf{r}, f)] + k^2(f)G(\mathbf{r}, f) = -4\pi\delta(\mathbf{R}). \quad (\text{A.9})$$

For $R \neq 0$ one obtains

$$\frac{d^2}{dR^2} [RG(\mathbf{r}, f)] + k^2(f)[RG(\mathbf{r}, f)] = 0 \quad (\text{A.10})$$

which has the trivial solution

$$G(\mathbf{r}, f) = \frac{1}{R} [A \cdot e^{-j \cdot k(f) \cdot R} + B \cdot e^{+j \cdot k(f) \cdot R}]. \quad (\text{A.11})$$

For $R \rightarrow 0$ the equation takes the form

$$\frac{1}{R} \frac{d^2}{dR^2} [RG(\mathbf{r}, f)] = -4\pi\delta(\mathbf{R}) \quad (\text{A.12})$$

with the solution

$$G(\mathbf{r}, f) = \frac{1}{R}. \quad (\text{A.13})$$

Adjusting the two solutions (A.12) and (A.14) yields

$$G(\mathbf{r}, f) = \frac{1}{R} [A \cdot e^{-j \cdot k(f) \cdot R} + (1 - A) \cdot e^{+j \cdot k(f) \cdot R}]. \quad (\text{A.14})$$

For a radiating source we expect only an outgoing wave. Hence, $A = 1$ and the solution for the radiated field is given by

$$\begin{aligned} \tilde{\mathbf{E}}(\mathbf{r}, f) &= \iiint G(\mathbf{r} - \mathbf{r}', f) \cdot \vec{F}(\mathbf{r}', f) d\mathbf{r}' \\ &= \iiint \frac{e^{-j \cdot k(f) \cdot |\mathbf{r} - \mathbf{r}'|}}{|\mathbf{r} - \mathbf{r}'|} \cdot \vec{F}(\mathbf{r}', f) d\mathbf{r}'. \end{aligned} \quad (\text{A.15})$$

In the far field $|\mathbf{r} - \mathbf{r}'| = |\mathbf{r}| = r$ and the field can be approximated by a spherical wave radiated from a localized source

$$\tilde{\mathbf{E}}(\mathbf{r}, f) = \frac{e^{-j \cdot k(f) \cdot r}}{r} \iiint \vec{F}(\mathbf{r}', f) d\mathbf{r}'. \quad (\text{A.16})$$

If we measure the field $\tilde{\mathbf{E}}_{\text{in}}(f)$ at a far-field distance $r = d_0$ from the source and the field $\tilde{\mathbf{E}}_{\text{out}}(f)$ at a distance $r = d + d_0$, then dividing any component of the two fields results in

$$\frac{\tilde{\mathbf{E}}_{\text{out}}(f)}{\tilde{\mathbf{E}}_{\text{in}}(f)} = \frac{d_0}{d + d_0} \cdot e^{-j \cdot k(f) \cdot d} \quad (\text{A.17})$$

leading to the transfer function given in (3).

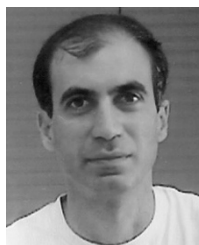
ACKNOWLEDGMENT

The authors acknowledge the help of The Samuel Neaman Institute for Advanced Studies in Science and Technology. The authors also thank Eng. A. Eichenbaum for useful discussions.

REFERENCES

- [1] H. T. Friss, "A note on a simple transmission formula," in *Proc. IRE*, vol. 34, 1946, pp. 254–256.
- [2] J. D. Kraus, *Antennas*. New York: McGraw-Hill, 1988.
- [3] R. K. Crane, "Propagation phenomena affecting satellite communication systems operating in the centimeter and millimeter wavelength bands," *Proc. of the IEEE*, vol. 59, no. 2, pp. 173–188, 1971.
- [4] —, "Fundamental limitations caused by RF propagation," *Proc. IEEE*, vol. 69, no. 2, pp. 196–209, 1981.
- [5] L. J. Ippolito, "Radio propagation for space communication systems," *Proc. IEEE*, vol. 69, no. 6, pp. 697–727, 1981.
- [6] H. J. Liebe, "Atmospheric EHF window transparencies near 35, 90, 140, and 220 GHz," *IEEE Trans. Antennas Propagat.*, vol. AP-31, no. 1, pp. 127–135, 1983.
- [7] R. A. Bohlander and R. W. McMillan, "Atmospheric effects on near millimeter wave propagation," *Proc. IEEE*, vol. 73, no. 1, pp. 49–60, 1985.
- [8] N. C. Currie and C. E. Brown, *Principles and Applications of Millimeter-Wave Radar*. Norwood, MA: Artech House, 1987.
- [9] H. J. Liebe, "An updated model for millimeter wave propagation in moist air," *Radio Sci.*, vol. 20, pp. 1069–1089, 1985.
- [10] —, "MPM—An atmospheric millimeter-wave propagation model," *Int. J. Infrared and Millimeter Waves*, vol. 10, no. 6, pp. 631–650, 1989.
- [11] H. J. Liebe, T. Manabe, and G. A. Hufford, "Millimeter-wave attenuation and delay rates due to fog/cloud conditions," *IEEE Trans. Antennas Propagat.*, vol. AP-37, pp. 1617–1623, Dec. 1989.
- [12] H. J. Liebe, G. A. Hufford, and T. Manabe, "A model for the complex permittivity of water at frequencies below 1 THz," *Int. J. Infrared and Millimeter Waves*, vol. 12, no. 7, pp. 659–675, 1991.
- [13] O. E. Delange, "Propagation studies at microwave frequencies by means of very short pulses," *Bell Syst. Tech. J.*, vol. 31, pp. 91–103, 1952.
- [14] M. P. Forrer, "Analysis of millimicrosecond RF pulse transmission," in *Proc. IRE*, vol. 46, 1958, pp. 1830–1835.
- [15] L. E. Vogler, "Pulse distortion in resonant and nonresonant gases," *Radio Sci.*, vol. 5, pp. 1169–1180, 1970.
- [16] G. I. Terina, "On distortion of pulses in ionospheric plasma," *Radio Eng. Electron. Phys.*, vol. 12, pp. 109–113, 1967.

- [17] D. B. Trizna and T. A. Weber, "Brillouin revisited: Signal velocity definition for pulse propagation in a medium with resonant anomalous dispersion," *Radio Sci.*, vol. 17, pp. 1169–1180, 1982.
- [18] C. J. Gibbins, "Propagation of very short pulses through the absorptive and dispersive atmosphere," *Proc. Inst. Elect. Eng.*, vol. 137, no. 5, pp. 304–310, 1990.
- [19] A. Maitra, M. Dan, A. K. Sen, S. Bhattacharyya, and C. K. Sarkar, "Propagation of very short pulses at millimeter wavelengths through rain filled medium," *Int. J. Infrared Millimeter Waves*, vol. 14, no. 3, pp. 703–713, 1993.
- [20] J. H. van Vleck, "The absorption of microwaves by oxygen," *Phys. Rev.*, vol. 71, pp. 413–424, 1947.
- [21] P. W. Rosenkranz, "Shape of the 5 mm oxygen band in the atmosphere," *IEEE Trans. Antennas Propagat.*, vol. AP-23, pp. 498–506, 1975.
- [22] H. J. Liebe, P. W. Rosenkranz, and G. A. Hufford, "Atmospheric 60 GHz oxygen spectrum: New laboratory measurements and line parameters," *J. Quantitative Spectroscopy and Radiative Transfer*, vol. 48, pp. 629–643, 1992.
- [23] F. Giannetti, M. Luise, and R. Reggiani, "Mobile and personal communications in the 60 GHz band: A survey," *Wireless Personal Communications*, vol. 10, pp. 207–243, 1999.
- [24] H. A. Kramers, "Some remarks on the theory of absorption and refraction of x-rays," *Nature*, vol. 117, p. 775, 1926.
- [25] R. de L. Kronig, "On the theory of dispersion of x-rays," *J. Opt. Soc. Amer.*, vol. 12, pp. 547–557, 1926.
- [26] A. Yariv, *Quantum Electronics*. New York: Wiley, 1988.



Yosef Pinhasi was born in Israel on May 3, 1961. He received the B.Sc., M.Sc., and Ph.D. degrees in electrical engineering from Tel-Aviv University, Tel-Aviv, Israel, in 1983, 1989, and 1995, respectively.

From 1983 to 1989, he worked with the Israeli Ministry of Defense as a Research and Development Engineer. Since 1990, he has been working in the field of electromagnetic radiation, investigating mechanisms of its generation in high power radiation sources and free-electron lasers (FELs). He developed a unified coupled-mode theory of

electromagnetic field excitation and propagation in the frequency domain, enabling study of wide-band interactions of electromagnetic waves in media in the linear and nonlinear (saturation) operation regimes. Currently, he is a Professor on the Faculty of Engineering at the College of Judea and Samaria, and the Head of the Department of Electrical and Electronic Engineering. He investigates utilization of electromagnetic waves in a wide range of frequencies for various applications such as communications, remote sensing, and imaging. The space-frequency approach, which he developed, is employed to study propagation of wide-band signals in absorptive and dispersive media in broad-band communication links, LANs, and wireless.



Asher Yahalom was born in Israel on November 15, 1968. He received the B.Sc., M.Sc., and Ph.D. degrees in mathematics and physics from the Hebrew University, Jerusalem, Israel, in 1990, 1991, and 1996 respectively.

From 1994 to 1998, he was Head of the Magnetostatic Team at Direx Medical System, working on the development of a novel MRI machine, he then became a Consultant in various mathematical and algorithmic issues related to the development of the "gamma knife"—a radiation-based head surgery system. In 1998, he joined the Israeli Free Electron Laser (FEL) Group, College of Judea and Samaria, Ariel, Israel, both as a Postdoctoral Fellow and as a Project Manager. Among his contributions to the project are theoretical contributions (finding Kramers–Kronig relations for FEL amplitude-phase, formulating a variational principle for FEL physics), technological contributions (working on two stage and multistage electron collectors, suggesting major improvement in the FEL Talbot effect radiation resonator which led to the first powerful lasing on April 9, 2003). Currently, he is a Senior Lecturer on the Faculty of Engineering, College of Judea and Samaria, where he is also the Founder and Academic Director of the FEL User Center. His research interests include works in a wide range of scientific and technological subjects ranging from the foundations of quantum mechanics to molecular dynamic, fluid dynamics, electromagnetics, communications, signal processing and imaging.



Oren Harpaz was born in Israel on May 19, 1976. He received the degree in electrical engineering from The College of Judea and Samaria, Ariel, Israel, in 2002. He is currently working toward the M.Sc. degree at Tel-Aviv University, Tel-Aviv, Israel. His thesis work is aimed at research of interactions between high power microwave and dielectric materials and study of the resulted heating in crystals.

Guy Vilner was born in Israel on October 24, 1977. He received the degree in electrical engineering from The College of Judea and Samaria, Ariel, Israel, in 2002.

He is currently working in his own company.